Effects of rain on Ku-band backscatter from the ocean

Robert F. Contreras
Department of Atmospheric Sciences, University of Washington, Seattle, Washington, USA

William J. Plant, William C. Keller, Kenneth Hayes, and Jeffrey Nystuen
Applied Physics Laboratory, University of Washington, Seattle, Washington, USA

Received 11 December 2001; revised 20 May 2002; accepted 3 March 2003; published 29 May 2003.

[1] During the Kwajalein Experiment (KWAJEX) in July and August 1999, measurements of the normalized radar cross section of the ocean, σ_o, were made at Ku-band with HH and VV polarizations from the R/V *Ronald H. Brown*. Data were collected at a variety of incidence angles during periods of rainfall as well as during clear conditions. During the experiment the rainfall rate ranged from 0 to 80 mm hr^{-1}. Coincident with the backscatter measurements, measurements of rain rate, wind speed, wind direction, and fluxes of heat and momentum were made. Since we were primarily interested in backscatter from the surface, we removed backscatter from the raindrops themselves for the σ_o measurements reported here. As a secondary result we show that the backscatter from the rain drops is a good indicator of rain rate. Most of the data were collected with the ship stationary and the bow held into the wind. Thus the azimuth angle between the antenna look direction and the direction from which the wind came was predominantly between 0° and 90°. Over this range, rain was found to increase σ_o at incidence angles of 30° to 75°, to have little effect near 20°, and to decrease σ_o very slightly between 14° and 16°. At all incidence angles, no discernible dependence of σ_o on wind speed was found during rainfall for wind speeds below 10 m s^{-1}; within experimental error the level of σ_o depended only on rain rate. For the lower incidence angles, this dependence was very small while at the higher incidence angles, σ_o depended on rain rate to a power that varied between about 0.5 and 1.2, being somewhat higher at large incidence angles and higher for HH polarization. The implication of these results is that rain produces small-scale surface displacements (wavelengths shorter than about 3 cm) that roughen the ocean surface much more than the wind for wind speeds below 10 m s^{-1}. The results also imply that when rain fills the entire scatterometer footprint on the surface and the wind speeds are low to moderate, scatterometry at Ku band is impossible. *INDEX TERMS:* 3360 Meteorology and Atmospheric Dynamics: Remote sensing; 3354 Meteorology and Atmospheric Dynamics: Precipitation (1854); 4504 Oceanography: Physical: Air/sea interactions (0312); *KEYWORDS:* microwave backscatter, rain, scatterometer, QuickSCAT, TRMM

Citation: Contreras, R. F., W. J. Plant, W. C. Keller, K. Hayes, and J. Nystuen, Effects of rain on Ku-band backscatter from the ocean, *J. Geophys. Res.*, *108*(C5), 3165, doi:10.1029/2001JC001255, 2003.

1. Introduction

[2] When raindrops hit the ocean surface, they change the properties of the surface, and therefore, the properties of microwave signals scattered from the surface. The synthetic aperture radar (SAR) images analyzed by [*Atlas*, 1994] give an impressive view of convective storms over the ocean. The author attributed specific features in the images, such as the echo-free hole and the bright center, to rain effects on the sea surface. *Melsheimer et al.* [1998] investigated SAR images of storms from the spaceborne imaging radar-C/X-band (SIR-C/X-SAR) missions in 1994 and found the images of storms to be different depending on the wavelength and polarization of the transmitted and received radar signal. The authors also found that rain impacting the ocean surface increased the backscatter at some wavelengths and incidence angles while decreasing it at others. Two spaceborne instruments in particular can be significantly affected by rain-induced changes in the ocean surface: the Tropical Rainfall Measuring Mission (TRMM) Precipitation Radar (PR) and the SeaWinds scatterometer on the QuikSCAT satellite. Both of these systems operate at Ku band (12.5–18 GHz) at low to moderate incidence angles in a backscattering mode. The TRMM PR, operating at incidence angles of 0° to 17°, is designed to determine rainfall as a function of altitude by measuring backscatter from raindrops. For these measurements to be accurate, attenuation of the microwave signal by rain in the atmosphere must be taken into account. Presently the differences between surface backscatter when

0148-0227/03/2001JC001255$09.00

rain is falling and when it is not are attributed completely to atmospheric attenuation. A change in surface backscatter due to rain will cause the calculated attenuation, and therefore the rain rates from the instrument to be in error. For SeaWinds, which determines wind speed and direction over the ocean from microwave return at incidence angles of 46° and 54°, rain changes the basic signal used for the measurement both by causing scattering and attenuation in the atmosphere and by changing scattering from the ocean surface. This paper reports results of measurements to determine the microwave backscattering cross section of the sea, σ_o, in the presence of rain at Ku-band and at low to moderate incidence angles. In order to isolate this signal from the backscatter from rain drops themselves, we remove the latter from the total signal on the basis of its Doppler shift. A secondary result of this procedure is to show that the signal from the rain drops is a good indicator of rain rate.

[3] Rain falling on the ocean surface has a multitude of effects that can alter the water surface and its scattering. The most noted is the droplet splash with its associated ring waves. When a raindrop impacts a water surface, it typically creates a crater with a crown that evolves into a vertical stalk. This is followed by radiating ring waves, which serve to enhance the surface wave spectrum. Photographs of this drop impact evolution are shown in Figure 1 and are given by [*Worthington*, 1963]. All of these splash products scatter microwave radiation but the contribution of each changes with incidence angle and polarization.

[4] In addition to the raindrop splash, the damping of gravity waves by rain is a phenomenon that has been long noted by mariners. *Tsimplis* [1992] discussed possible mechanisms for wave damping and concluded from laboratory experiments that rain induced subsurface turbulence dominates the damping, with the effect being greatest for the shortest waves. *Nystuen* [1990] suggested that this turbulence could be modeled by an eddy viscosity which increases viscous damping above the ordinary molecular rate. *Yang et al.* [1997] performed laboratory experiments in a wind-wave tank with artificial rain and identified both wave generation and damping by rain.

[5] *Capolino et al.* [1997] used a full wave scattering model to predict microwave scattering from the sum of wind wave and ring wave spectra. They calculated that near nadir, σ_o decreases with rain rate and that the magnitude of the decrease was greater than 3 dB at their highest simulated rain rates. The first work performed at scatterometer incidence angles to determine the effect of rain on backscatter was that of *Moore et al.* [1979]. Using a wind-wave tank and an artificial rain generator they measured significant increases in Ku-band backscatter at 40° incidence at low winds. *Hansen* [1986] performed laboratory experiments without wind to investigate backscatter associated with 4-mm-diameter droplet impacts with a 9-GHz microwave system at incidence angles ranging from 8° to 45°. He concluded that for the entire range of incidence angles, VV polarized radiation scattered from all of the features of the splash while HH polarized radiation scattered primarily from the stalk. *Wetzel* [1990] modeled scattering from isolated rain drop splash products and then expanded these results using statistical models for surface slopes and stalk height distributions to emulate real world conditions. He concluded that the major scattering feature is the stalk and that the contribution from the ring waves is small and dependent upon polarization. *Sobieski et al.* [1999] synchronized high-speed, digital photography with a VV polarized Ku-band system at a 30° incidence angle to analyze backscatter that is associated with the various phases of a drop splash. They found that ring waves are the dominant scatterers at this incidence angle and frequency. These results can be reconciled with those of Wetzel by noting that although the instantaneous backscatter is greater from the stalk, its lifetime is much less than that of ring waves. The maximum lifetime of a stalk from a drop 2.5 mm in diameter is less than 150 ms, whereas the corresponding ring waves last at least 400 ms and sometimes longer than 1500 ms.

[6] To better explain how ring waves increase the Backscatter, it is useful to introduce Bragg scattering. Bragg scattering is the scattering phenomenon utilized by scatterometers and attributed to backscatter from ring waves during rain. It occurs when the path difference of radiation impinging on successive identical phases of surface waves is equal to the wavelength of the transmitted and received radiation. With Bragg scattering the transmitted radiation scatters back towards the antenna even at large incidence angles which would not be the case with simple specular scattering. The Bragg resonance condition can be expressed as

$$\lambda_B = \frac{\lambda_\circ}{2 \sin \theta}, \tag{1}$$

where λ_B is the wavelength of the surface wave, $\lambda_\circ$ is the wavelength of the transmitted radiation, and θ is the incidence angle. Since the wavelengths of ring waves span millimeters to centimeters, they satisfy the Bragg resonance condition (equation (1)) for Ku-band radiation over a wide range of incidence angles. Therefore the effect of rain on the surface wave field should be reflected in its effect on the backscatter.

[7] In order to better quantify the return from ring waves, *Bliven et al.* [1997] extended the theory of *Méhauté* [1988] for single drops by modeling the surface wave spectrum associated with impacts of many drops as a log-Gaussian and found that the model agreed well with laboratory experiments. Working in a wind-wave tank and using an artificial rain maker, *Braun et al.* [1999] investigated the effect of rain on X-band backscatter for incidence angles of 28°, 40°, and 55°. They determined that ring waves were the primary scatterer for VV polarized radiation at all of these incidence angles but that ring waves dominated HH polarized backscatter only at 28°. As the incidence angle increased, the contribution from ring waves decreased while backscatter from the nonpropagating splash products, such as the crown and stalk, increased. In addition, *Gade et al.* [1998] showed that at low wind speeds and 28° incidence angle rain induced ring waves are the dominate scatters of copolarized (HH and VV) backscatter, thereby eliminating the azimuthal dependence of the backscatter.

[8] The laboratory experiments and modeling studies outlined above have provided insight into the effects of rain on Ku-band backscatter from the ocean surface. However, real world conditions that are difficult, if not impossible, to reproduce in wind-wave tanks may substan-

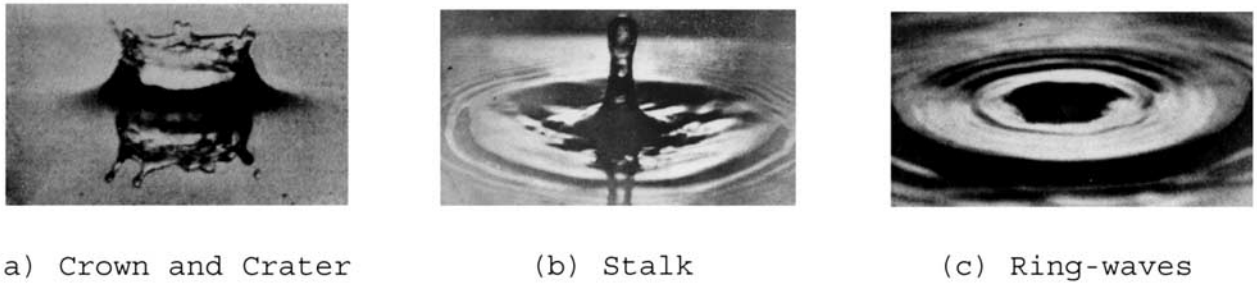

Figure 1. Splash products when a raindrop falls onto a water surface. The figures are reproductions of photographs from *Worthington* [1963].

tially affect the results. For example, the steepness of the wind waves, which depends on fetch, may be important for determining the wave numbers that are enhanced and those that are damped. In wave tanks, the fetch is usually limited to less than 30 m. Furthermore, the fall velocity of the impinging drops has been shown by *Sobieski et al.* [1999] to be important in creating splash products. In order for the drops to approach terminal fall velocity, they must fall at least 10 m, a condition difficult to produce in the laboratory. Furthermore, a realistic drop size distribution may also be crucial to investigating rain effects on backscatter.

[9] The field study of *Smith et al.* [1998], using an S-band radar at the low grazing angle of 4°, showed the importance of ring waves on the backscatter by demonstrating their signature in Doppler spectra. However, the results are difficult to extrapolate to higher microwave frequencies and lower incidence angles. The data reported in this paper illuminate the effects of rain on Ku-band backscatter from the ocean surface in a natural setting and at a variety of incidence angles relevant to spaceborne sensors.

2. Data Collection

[10] The TRMM Kwajalein Experiment (KWAJEX) took place July and August 1999 and was based at the Kwajalein Atoll Missile Range in the Marshall Islands (8°N, 167°E). During the experiment, Ku-band microwave backscatter from the ocean surface was measured at a range of incidence angles overlapping the operational incidence angles used by the QuikSCAT scatterometer and the TRMM PR. These measurements were taken coincident with measurements of rain rate, wind speed and direction, and fluxes of heat and momentum in order to quantify the dependence of backscatter on rain rate and 10-m neutral wind vector.

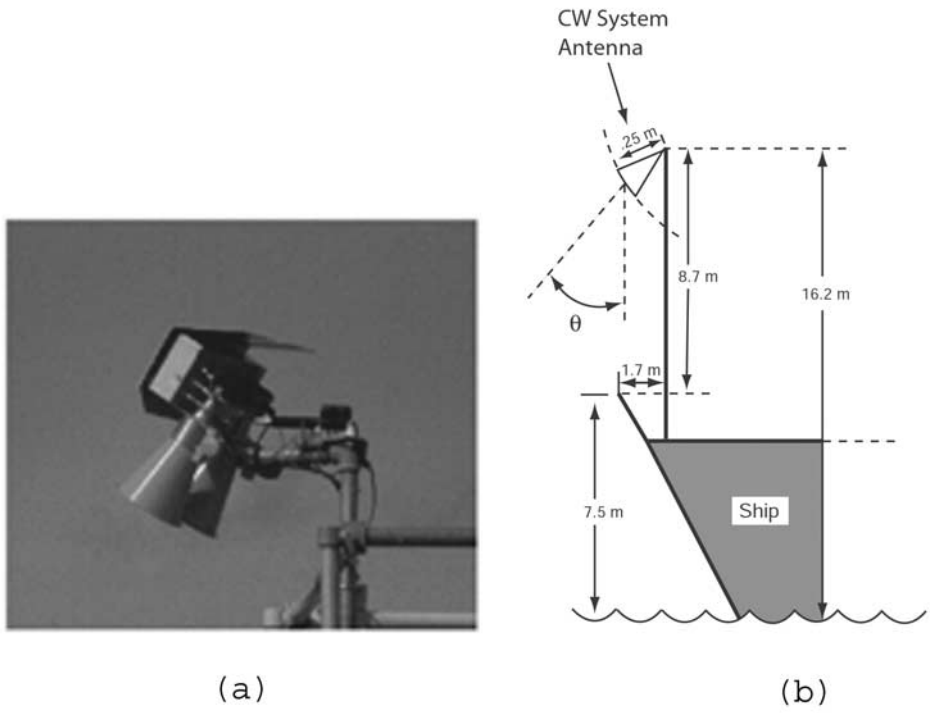

Figure 2. The CW Ku-band system aboard the NOAA ship *Ronald H. Brown*. (a) Photograph of the horn antennas used on the ship. (b) Illustration of the system setup.

2.1. Ku-Band Microwave System

[11] Backscatter was measured by the Ku-band microwave system shown in Figure 2a. It was operated from atop a platform on the bow of the NOAA ship *Ronald H. Brown*. The system was 16.2 m above the ocean surface and looked to the port side at a 55° azimuth angle to the bow. It operated at 14 GHz (Ku-band) and was a continuous-wave, dual-polarized, coherent system. It stepped through incidence angles providing data at angles ranging from 13.5° to 80°. Figure 2b shows the configuration of the system.

[12] Backscattered fields were sampled at 2048 Hz; mean received power was computed every 1024 samples (0.5 s) and recorded. This was done for both horizontal transmit and receive (HH) and vertical transmit and receive (VV) polarizations. Since the system was coherent, it was possible to compute the Doppler spectra of the returned signal. Backscatter from objects stationary with respect to the antenna, such as the deck of the ship, was filtered out of the signal by removing return with zero Doppler shift. Mean Doppler spectra were recorded for both polarizations every 40 records (or 20 s). A time stamp corresponding to the final record used to compute the mean spectrum was recorded with the data. Examples of these spectra for VV polarization are shown in Figure 3 for a case with rain and a case without.

[13] The radar equation can be solved for σ_o, giving

$$\sigma_\circ = C_{cw}\left(\frac{r^4}{A}\right)\left(\frac{P_r}{P_t}\right), \tag{2}$$

where A is the illuminated area of the system,

$$A = \frac{\pi}{4}\frac{\Phi_h \Phi_v h^2}{\cos^3\theta}. \tag{3}$$

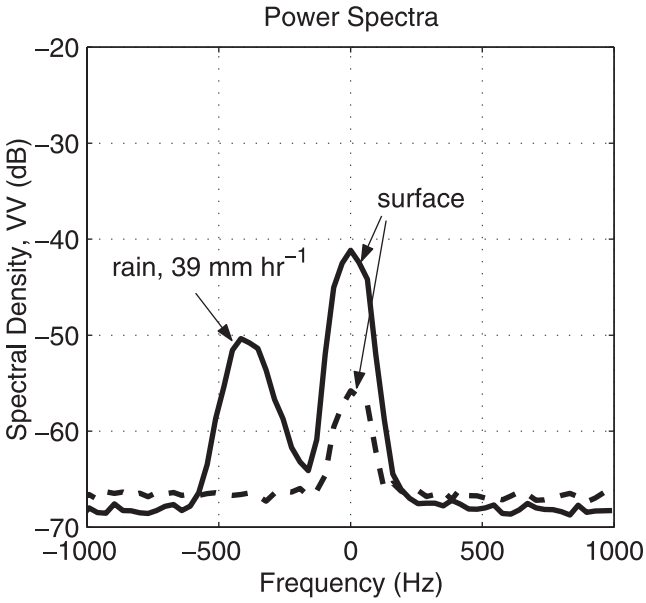

Figure 3. Doppler spectra of the VV received power for a case with rainfall (solid line) and a case without rain (dashed line). For the raining case, $\theta = 48°$, $U_{10} = 5.2$ m s^{-1}, and $\chi = 86°$; for the nonraining case, $\theta = 49°$, $U_{10} = 5.5$ m s^{-1}, and $\chi = 81°$.

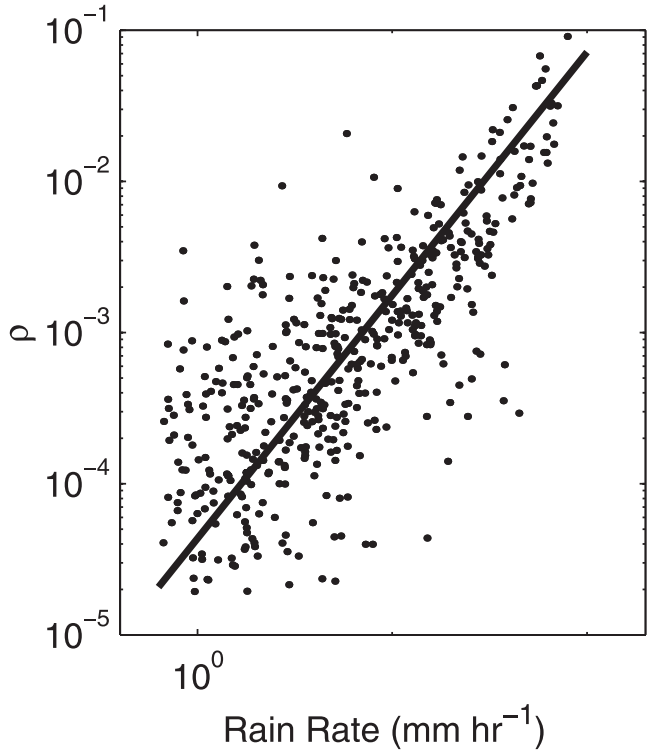

Figure 4. Fraction of backscatter due to rain divided by illuminated volume versus rain rate. The least squares fit to the function $\rho = aR^b$ where the rain rate R is shown as the solid line. The coefficients $a = 4.4 \times 10^{-5}$ and $b = 1.6$ give an $r^2 = 0.89$.

C_{cw} is a calibration constant, r is the distance to the illuminated area. Φ_h and Φ_v are one-way, half-power full horizontal and vertical beamwidths, h is the height of the system above the surface, and θ is incidence angle. The

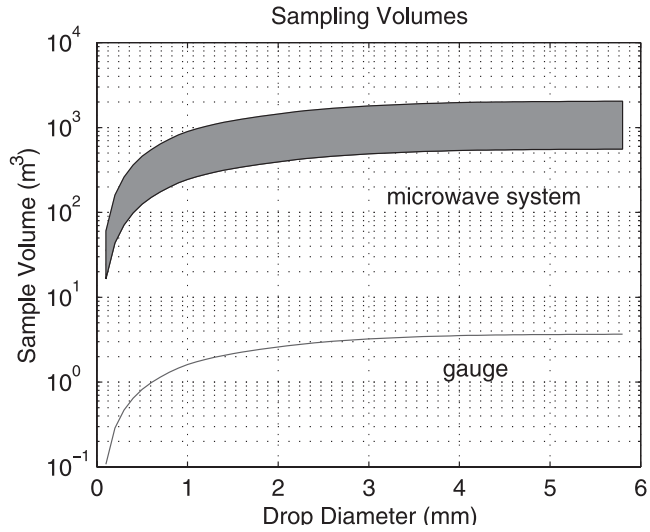

Figure 5. Sampling volumes of the CW system and the Hasse rain gauge, using $A = \frac{\pi}{4}\left[\frac{\Phi_V \Phi_H h^2}{cos^3(\theta)}\right]$ for the CW system and $A = 200$ cm^2 for the Hasse rain gauge. With the terminal fall speed v_t from *Gunn and Kinzer* [1949] and averaging time $T = 20s$, the sampling volumes are $V = Av_tT$.

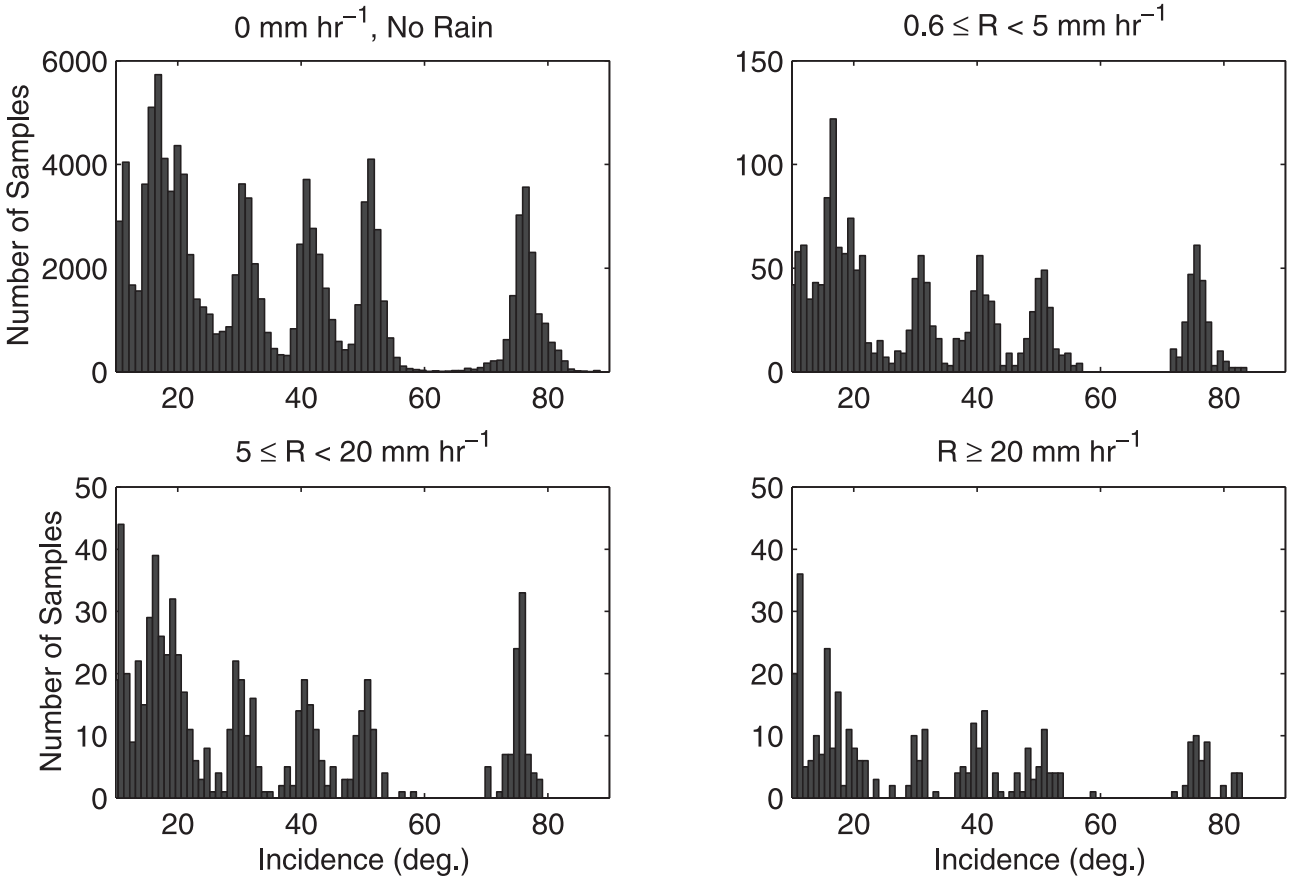

Figure 6. Histograms of the incidence angles, θ, at which data were taken during KWAJEX. The incidence angle range of the histogram is 10° to 90°. The different panels show the number of data samples in the rain rate bins: 0 mm hr^{-1} (no rain), $0.63 \leq R < 5$ mm hr^{-1}, $5 \leq R < 20$ mm hr^{-1}, and $R \geq 20$ mm hr^{-1}. These histograms do not reflect restrictions in azimuth angle nor the additional filtering at 76°.

beamwidths (Φ_h, Φ_v) in degrees were (6.8, 6.4) at HH and (6.9, 6.4) at VV polarization. The calibration constant, C_{cw} accounts for the antenna gain as well as the wavelength of the transmitted signal. The constant was determined before the experiment by measuring the returned power from corner reflectors of known cross section. We estimate the uncertainty in the calibration to be about 1 dB.

[14] Since the CW system was coherent and falling raindrops usually had a significant component of velocity in the direction of the antenna, it was possible to remove scattering from the raindrops from the total return. To isolate the surface scattering and remove that due to rain, all backscatter with Doppler shifts greater than 130 Hz was removed. This corresponded to removing backscatter from objects with radial velocities greater than 1.4 m s^{-1}. Since the velocity spread from Bragg waves was shown by *Plant et al.* [1994] to be less than 0.6 m s^{-1} and the ship's velocity was small, ~0.2 m s^{-1}, this velocity limit was sufficiently high to include all the surface scattering while excluding the falling drops in most cases. When the antenna had an incidence angle of ~76° this procedure was not always effective, since rain had the greatest probability of falling nearly perpendicular to the antenna look direction, yielding small radial velocities and a signal difficult to separate from the surface signal. At this incidence angle, each spectrum was inspected and only data which had a separable rain signal were used.

[15] The proximity of the CW system to the surface assured that very little attenuation occurred due to rain in the atmosphere between the antenna and the surface. For rain with a mass-weighted mean radius of 1.5 mm, a rain rate of 150 mm hr^{-1}, and using the *k-Z* relations shown by *Haddad et al.* [1995], the attenuation is 0.2–0.3 dB for incidence angles up to 51°. This is within the error of the measurements, and therefore attenuation was ignored. At an incidence angle of ~76° and this high rain rate, the attenuation is 0.72 dB, so that measurements at this angle in heavy rain may be somewhat affected by attenuation.

[16] A side effect of the necessity of removing the signal from raindrops from the sea return was the easy determination of the level of the rain signal. Integrating spectra over the frequency regions away from the surface scatter and dividing by the total spectral integral then multiplying by the ratio of the received to transmitted power yielded a dimensionless measure of the return from raindrops. Dividing this by the volume within the illumination cone yields a measure (ρ) of backscatter from the raindrops that is

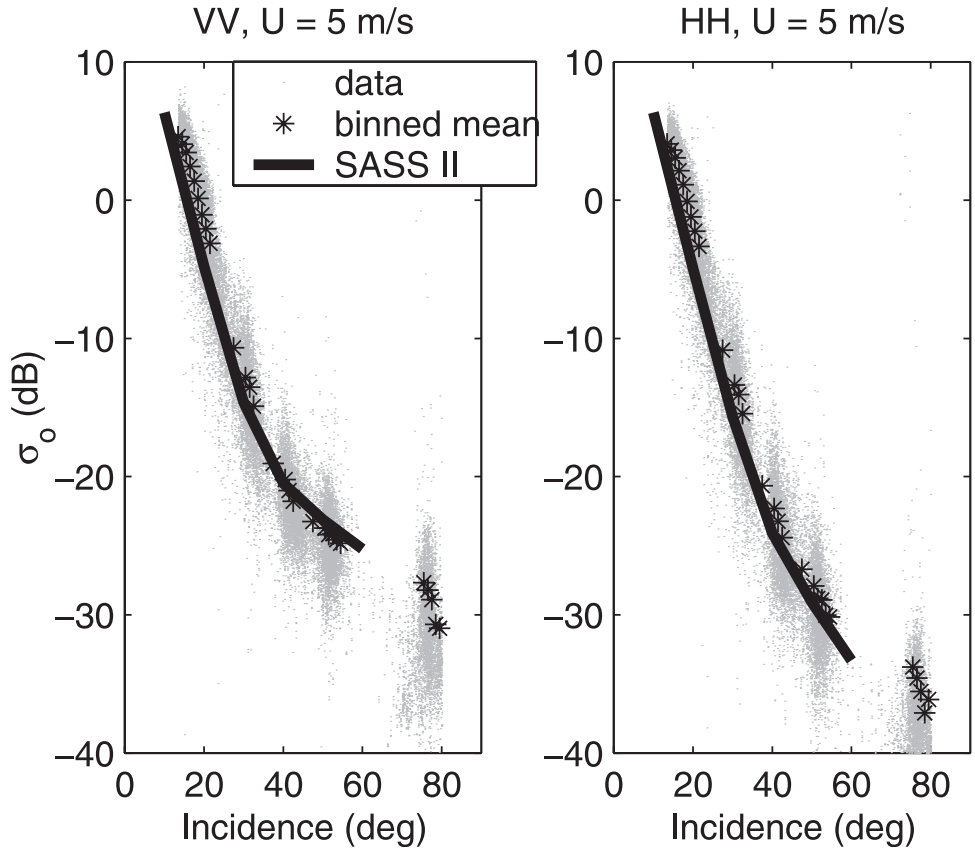

Figure 7. The normalized radar cross section, σ_o versus incidence angle. Data collected during KWAJEX are plotted along with their binned means and the SASSII model function weighted by the measured azimuth angle distribution.

independent of the incidence angle. This quantity is related to the traditional effective reflectivity factor and as can be seen in Figure 4, was well related to the rain rate.

2.2. Hasse Rain Gauge

[17] Rain rate was obtained from a Hasse rain gauge. The Hasse gauge is a catch bucket system that has both horizontal and vertical collection surfaces. The vertical surfaces are meant to catch raindrops with large horizontal components of velocity and to minimize flow distortion. Rain rate data are often corrupted by flow distortion and large horizontal velocities on moving ships. The instrument is described and its measurements verified by *Hasse et al.* [1998]. During KWAJEX, rain rate data from the Hasse gauge were recorded every 10 s and corrected for the environmental wind speed. It is standard to average the rain data over at least 2 min to address sampling variability issues. However, in the following analysis, 20-s averages from the Hasse rain gauge were used. Using shorter time periods for the rain rate averages, 20 s as opposed to 120 s, introduces significant sources of uncertainty: a time delay in the measurements and a possible undersampling of the drop size distribution. The time delay results from the fact that the gauge is a catch bucket system and needs to be wet before measurements can be made. The undersampling results from the small volume of the rain sampled by the Hasse gauge. The concern here is whether the rain rate measured by the gauge is representative of the rain that strikes the area illuminated by the CW system in the data collection period. The sampling volumes of both instruments are shown in Figure 5. When considering a 2-mm-diameter drop and 20 s collection period, the sampling volume for the CW system ranges from $\sim$400 m^3 to $\sim$1500 m^3 depending on the incidence angle, whereas the sampling volume of the rain gauge is $\sim$2.5 m^3. For a given rain rate a Hasse gauge may not catch the largest drops in a drop size distribution and thus underestimate the rain rate. Undersampling is especially a problem at low rain rates. Compounding this is the physical separation of the rain gauge and the microwave system footprint; the rain sampled in the two locations may simply be different. The difference in sampling of the two instruments is the largest source of uncertainty in the analysis. One remedy for this situation would have been to allow the gauge to collect rain for longer times and take longer means of the backscatter. The length of time the CW system spent at any one incidence angle varied. The period was chosen with the purpose of getting adequate backscatter samples at a range of incidence angles during rain. Unfortunately, the sampling period of the coincident rain measurements was not considered and the system only spent 20 to 100 s per incidence angle. In order to have a consistent averaging period and maximize the amount of data used, 20 s averaging periods were used with more uncertainty in the rain gauge data. The Hasse rain gauge measures the rain rate by counting the number of calibrated drops that pass a sensor. The drops have a mass of

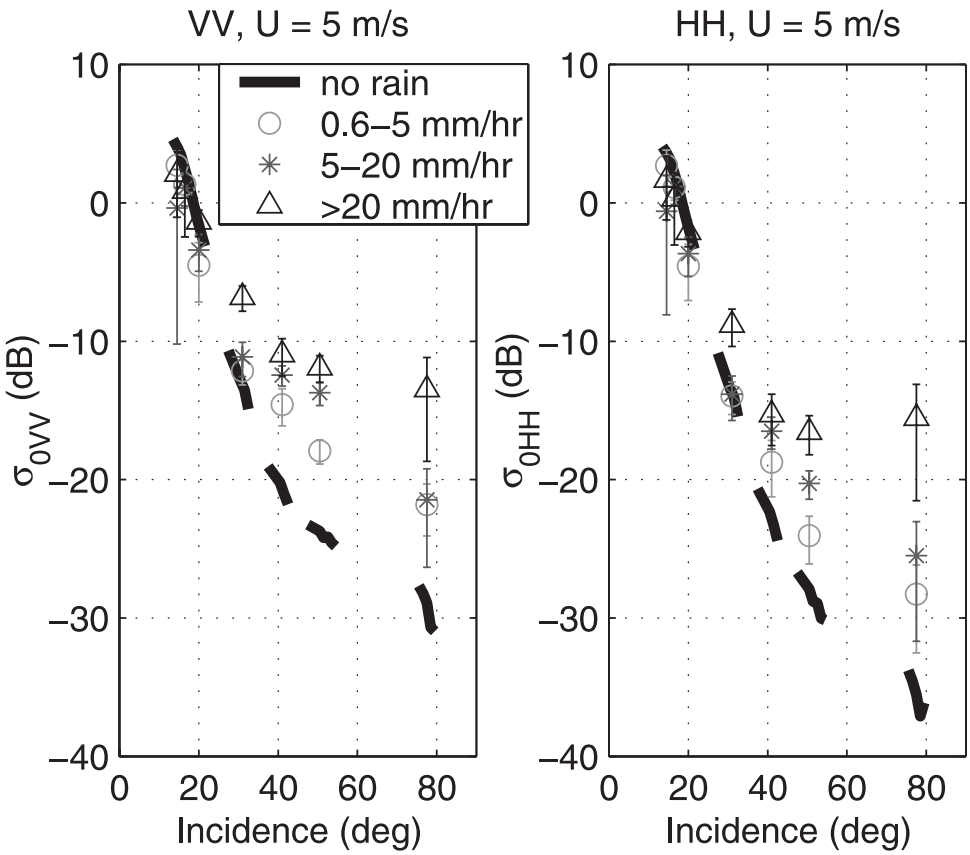

Figure 8. The normalized radar cross section, σ_o versus incidence angle for no rain (solid line), and rain rates of 0.63–5 mm hr^{-1}, 5–20 mm hr^{-1}, and ≥20 mm hr^{-1}. Error bars represent the 95% confidence limits.

0.1 g which corresponds to a rain drop of 2.2 mm in diameter. The minimum rain rate used in the following analysis is that which has one 2.2 mm droplet per sampled volume. Using terminal fall speeds from *Gunn and Kinzer* [1949] to compute the sampling volumes, which are shown in Figure 5, and assuming the Marshall-Palmer drop size distribution [*Marshall and Palmer*, 1948], the minimum rain rate was determined to be 0.63 mm hr^{-1}.

2.3. Neutral Winds at 10 m

[18] It is standard to express surface winds as the neutral stability winds at 10 m height, denoted U_{10}. This enables winds measured at different heights under different stability conditions to be compared. In order to convert the winds measured on the *Ronald H. Brown* to the neutral winds at 10 m, Monin-Obukhov (MO) similarity theory was used. MO similarity theory states that within the atmospheric surface layer

$$\frac{\partial \bar{u}}{\partial z} = \frac{u_*}{kz}\phi_m(\zeta). \tag{4}$$

In other words, the change in the mean wind speed with height $\frac{\partial \bar{u}}{\partial z}$ is proportional to the momentum flux u_*, and inversely proportional to the position in the layer z, with all of this being multiplied by a function accounting for the stability of the layer, $\phi_m(\zeta)$; ζ is the nondimensional height,

$$\zeta = \frac{z}{L},$$

where

$$L = \frac{-u_*^3}{kB_0}$$

is the Obukhov length with $k = 0.4$ being the von Karman constant and B_0 the buoyancy flux. The Obukhov length gives a measure of the stability of the layer; it is roughly the height at which the turbulent kinetic energy (TKE) produced by buoyancy becomes comparable to that produced by shear. An assumption of MO similarity theory that has proven to be accurate over land is that within the surface layer the fluxes of heat and momentum are constant. Much effort has been put into determining the functional form of $\phi_m(\zeta)$. The most accepted form is outlined by *Businger et al.* [1971] and *Dyer* [1974]. From this point on, this function will be referred to as the Businger-Dyer stability relation. Now equation (4) can be integrated with respect to height to give the mean wind speed $\bar{u}$ at a specific height z under neutral conditions. Upon integration the equation becomes

$$\bar{u}(z) = \frac{u_*}{k}\left[\ln\left(\frac{z}{z_0}\right) - \Psi_m(\zeta)\right]. \tag{5}$$

Here the constant of integration, z_0, the roughness length, accounts for the fact that $\frac{\partial \bar{u}}{\partial z}$ is finite at $z = 0$. The value of z_0

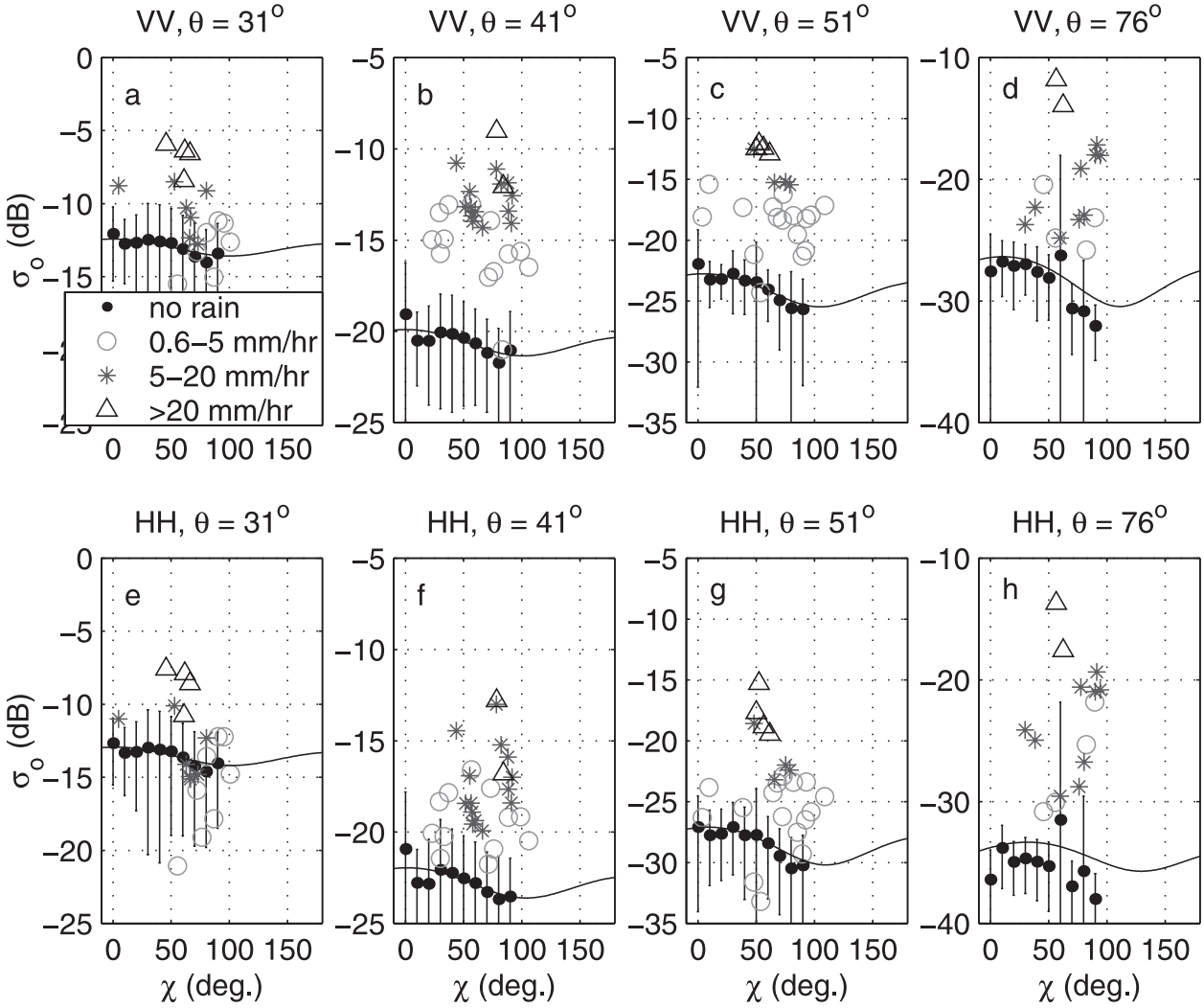

Figure 9. Dependence of the cross section, σ_o, on the azimuth angle, χ, for no rain, 0.63–5 mm hr^{-1}, 5–20 mm hr^{-1}, and $\geq$20 mm hr^{-1}. The nonraining means and standard deviations are computed for 10° bins in azimuth. In addition, the model function (equation (8)) is fit to the nonraining data.

is loosely related to the roughness of the bottom boundary. If $x = (1 - \gamma_1\zeta)^{\frac{1}{4}}$,

$$\Psi_m(\zeta) = \int_0^{\zeta} \frac{\phi_m(\zeta')}{\zeta'} d\zeta'$$
$$= \ln\left(\left(\frac{1+x^2}{2}\right)\left(\frac{1+x}{2}\right)^2\right) - 2\tan^{-1}(x) + \frac{\pi}{2}$$
$$\text{for } -2 < \zeta < 0 (\text{unstable}), -\beta\zeta \text{ for } 0 \leq \zeta (\text{stable}), \quad (6)$$

is the integrated Businger-Dyer stability relation with γ_1 = 16 and β = 5 being constants that have been deduced from various field experiments outlined by *Garratt* [1992].

[19] The 10-m neutral stability winds used in this analysis were calculated using measurements of the mean wind speed and direction from the Improved Meteorological Measurements for Buoys and Ships (IMET) sensors and flux measurements provided by the NOAA Environmental Technology Laboratory's (ETL) Air Sea Interaction Group. The IMET package, manufactured by the Woods Hole Oceanographic Institution, includes a rain gauge and sensors to measure wind speed, wind direction, temperature, humidity, and short-wave radiation. The wind speed and direction were recorded every 10 s. The wind measurement assigned to a measured cross section was that made most recently prior to its recorded time. The NOAA ETL group operated a suite of instruments on the bow of the ship that measured many quantities including the fluxes of heat and momentum. The flux data were provided as 10-min averages which were linearly interpolated to coincide with the σ_o data times. Using the mean wind speed, $\bar{u}$ measured at 14.12 m height, the flux of heat, and the flux of momentum, U_{10} can be computed. Evaluating equation (5) at z = 14.12 m and z = 10 m and eliminating z_0, we arrive at the relation

$$U_{10} = \bar{u}(14.12) - \frac{u_*}{k}\left[\ln\left(\frac{14.12}{10}\right) - \Psi\left(\frac{14.12}{L}\right) + \Psi\left(\frac{10}{L}\right)\right], \quad (7)$$

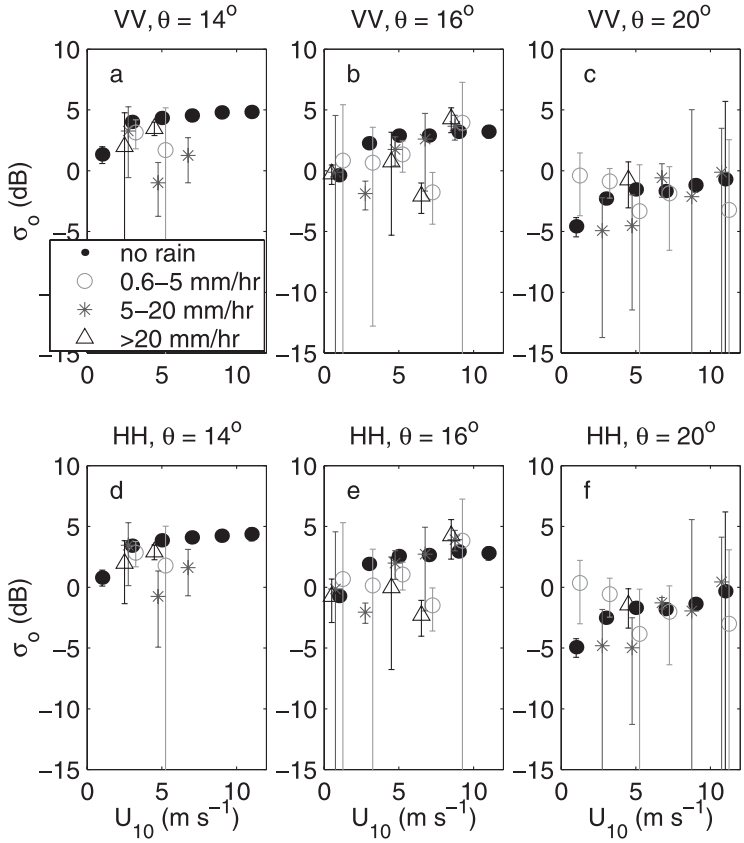

Figure 10. The dependence of σ_o on U_{10} of the for the lower incidence angles: 14°, 16°, and 20°. Error bars represent the 95% confidence limits. The mean cross sections during rain have been offset in U for ease of viewing: $0.63 \leq R < 5$ mm hr^{-1} has been shifted 0.25 m s^{-1}, $5 \leq R < 20$ mm hr^{-1} has been shifted -0.25 m s^{-1}, and $R \geq 20$ mm hr^{-1} has been shifted -0.50 m s^{-1}.

which was used to compute the 10-m neutral winds in this analysis.

3. Results

[20] Ku-band backscatter, as represented by σ_o, is a function of incidence angle, θ; polarization; 10-m neutral wind speed, U_{10}; the angle, χ, between the direction from which the wind comes and the antenna look direction; and a rain characteristic. The rain characteristic used in this analysis is the rain rate, R, because it is commonly used and intuitive. We note, though, that this may be an incomplete specification of the rain since the drop size distribution could also affect the backscatter. In this section, the effects of rain on σ_o will be presented as a functions of the above quantities: θ, polarization, χ, U_{10}, and R.

3.1. Dependence of Cross Section on Incidence Angle

[21] During KWAJEX, σ_o was measured at incidence angles that ranged from about 0° to 80°. Figure 6 is a histogram of the incidence angles at which measurements were made for the rain rate bins: 0 mm hr^{-1} (no rain), $0.63 \leq R < 5$ mm hr^{-1}, $5 \leq R < 20$ mm hr^{-1}, and $R \geq 20$ mm hr^{-1}. Although data were collected at incidence angles less than 13.5°, data in this range were not considered because the transmitted and received radiation were obstructed by the ship. Since any fixed signal was filtered from the recorded data, the effect was a shadowing of the ocean surface. Since the system stepped through incidence angles, certain angles were emphasized. These angles were approximately 16°, 20°, 31°, 41°, 51°, and 76°. We will use these angles, with the addition of 14° as the basis for incidence angle bins in the following analysis.

[22] The dependence of σ_o on incidence angle for 10-m neutral wind speeds between 4 m s^{-1} and 6 m s^{-1} in nonraining conditions is shown in Figure 7, along with the SASSII model [*Wentz et al.*, 1984]. The figure shows individual VV and HH polarization cross sections and their means in 1° bins in incidence angle, and the SASSII model function. The data presented here correspond to $0° < \chi < 90°$, with the model function being weighted by the azimuthal distribution of our data. The general agreement between the model function and the data was validation that the CW system was working correctly and that flow distortion around the ship was not a major problem. In order to remove a slight mismatch of VV and HH polarization data at low incidence angles, we adjusted our cross sections so that the ratio of VV to HH data at the 20° incidence angle for wind speeds of 5 m s^{-1} were the same as those of the SASSII model function. The adjustment lowered σ_o for VV polarization by 0.73 dB and increased that for HH by 0.73 dB.

[23] The same 1° binned mean cross sections are plotted as solid black lines in Figure 8. Also plotted in the figure are cross sections measured for three rain rate intensities: 0.63–

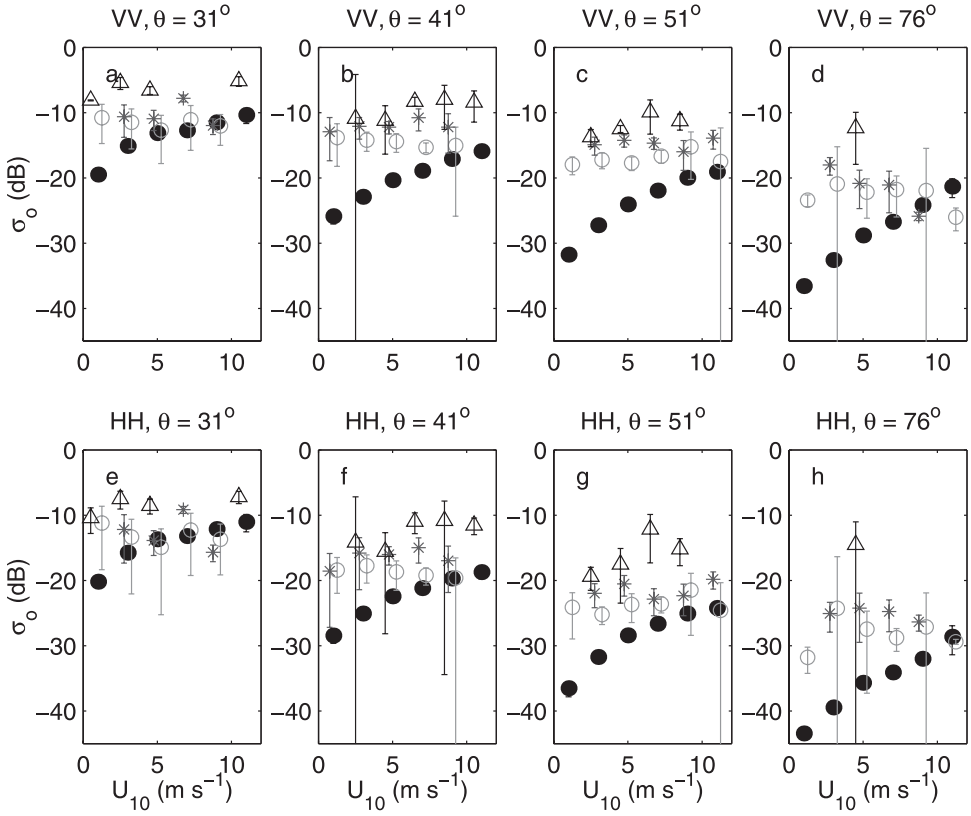

Figure 11. The dependence of σ_o on U_{10} of the for the higher (scatterometer) incidence angles: 31°, 41°, 51°, and 76°. The symbols are the same as in Figure 10. Error bars represent the 95% confidence limits. The mean cross sections during rain have been offset in U for ease of viewing: $0.63 \leq R < 5$ mm hr^{-1} has been shifted 0.25 m s^{-1}, $5 \leq R < 20$ mm hr^{-1} has been shifted -0.25 m s^{-1}, and $R \geq 20$ mm hr^{-1} has been shifted -0.50 m s^{-1}.

5 mm hr^{-1}, 5–20 mm hr^{-1}, and ≥20 mm hr^{-1}. The width of the incidence angle bins was 2° for $\theta < 20°$ and 5° for $\theta > 20°$. The error bars represent the 95% confidence interval of the binned means. It is obvious from the figure that rain alters σ_o. At low incidence angles, less than ∼20°, rain appears to decrease σ_o; however, few of the data show statistically significant decreases. This lack of significance at low incidence angles may be due to the small sample size, the complexity of the scattering mechanism, or both. At incidence angles greater than ∼30° the effect of rain is to increase σ_o; the magnitude of this change increases with incidence angle and with rain rate. It should also be kept in mind that data at 76° have the additional restraint that the rain signal be separable from the surface signal. This condition reduces the sample sizes: N = 26 for rain rates of 0.63–5 mm hr^{-1}, N = 19 for rain rates of 5–20 mm hr^{-1}, and N = 5 for rain rates ≥20 mm hr^{-1}.

[24] The range of incidence angles between ∼20° and ∼30° is a transitional region where rain has little effect. This crossover region corresponds to Bragg wavelengths from 2.1 to 3.1 cm and provides a natural division to the analysis of this data. *Melsheimer et al.* [1998] found a similar, although longer, transition occurring at about 10 cm which corresponds to an incidence angle of about 6 degrees for Ku band. The difference in the crossover wavelength between this study and that of *Melsheimer et al.* [1998] may be associated with uncertainties inherent to SAR data. Other studies from a near-surface scatterometer (M. Gade, personal communication, 2002) suggest a transitional wavelength of about 4 cm, which is in much better agreement with these data. Here results will be presented first, for the low incidence angles: 14°, 16°, and 20°, and then for the higher incidence angles: 31°, 41°, 51°, and 76°.

3.2. Cross Section Versus Azimuth Angle

[25] During the experiment the crew made an effort to keep the ship pointed into the wind. As a result, 97% of the data were collected for $0° < \chi < 90°$, 58% for $40° < \chi < 70°$. Relative to the ship, $\chi = 0°$ is 55° to the port (left of the bow) and $\chi = 90°$ is 35° to the starboard (right of the bow). In order to minimize possible flow distortion from the ship, only winds for which $0° < \chi < 90°$ are used in this analysis. Arranged according to incidence angle, the dependence of σ_o on χ measured at KWAJEX is shown in Figure 9. The cross sections in this figure had corresponding wind speeds of 5 ± 0.5 m s^{-1}. The solid points are σ_o means for nonraining conditions and the error bars represent the corresponding standard deviations. The solid line is a linear least squares fit of the nonraining data to the model function,

$$\sigma_\circ = A_0 + A_1 \cos\chi + B_1 \sin\chi + A_2 \cos 2\chi + B_2 \sin 2\chi. \quad (8)$$

[26] Even though the least squares fit picks out the azimuthal dependence at higher incidence angles typically

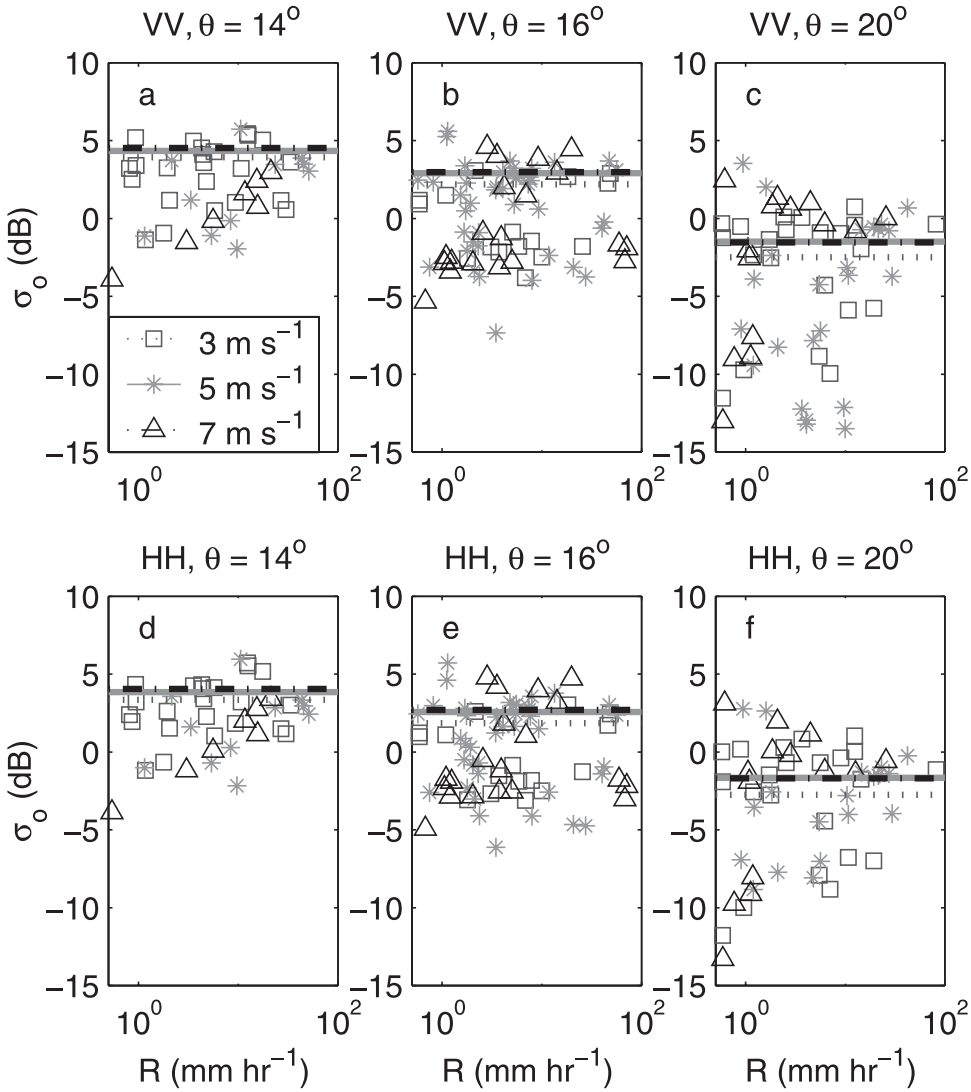

Figure 12. The cross section as a function of rain rate for wind speed bins: 2 m $s^{-1} \leq U_{10} < 4$ m s^{-1} (squares), 4 m $s^{-1} \leq U_{10} < 6$ m s^{-1} (asterisks), and 6 m $s^{-1} \leq U_{10} < 8$ m s^{-1} (triangles). Horizontal lines are the nonraining means for bins: 2 m $s^{-1} \leq U_{10} < 4$ m s^{-1} (dotted line), 4 m $s^{-1} \leq U_{10} < 6$ m s^{-1} (solid line), and 6 m $s^{-1} \leq U_{10} < 8$ m s^{-1} (dash-dotted line).

associated with scatterometers, with a maximum at ~0° and a minimum at ~90°, the measured standard deviations are much greater than those measured by *Plant et al.* [1998], and much greater than the peak to peak differences of the fitted model function. Therefore we have little confidence in determining the azimuthal effect of rain from the KWAJEX data. The reason for the variation in σ_o at any one azimuth angle is probably a result of the system being fixed with respect to the ship. In other work, when the azimuthal dependence of σ_o has been detected, the ocean has been illuminated at different azimuth angles almost simultaneously. This insured the same atmospheric conditions for all of the measurements. Since the system was fixed during KWAJEX it was necessary for the wind to change directions in order to collect data at different azimuths. As a result, the atmospheric conditions could have been quite different for different azimuths. Even though the conversion to neutral winds is an effort to account for the differences, the process itself is based on assumptions that may not be completely valid over the ocean. One assumption is that Monin-Obhukov (MO) similarity theory sufficiently describes the structure of the marine surface layer, and another is that the functions accounting for stability in MO, the Businger-Dyer relations, which were measured over land, are correct over the ocean. There is evidence that both of these assumptions are not entirely applicable [*Miller et al.*, 1997; *Plant et al.*, 1998]. Since considerable uncertainty exists in the azimuthal dependence of the cross section and the typical variation in azimuth is small compared to the rain effects, the dependence of the cross section on azimuth angle will be disregarded and the data will simply be binned for $0° < \chi < 90°$.

3.3. Cross Section Versus Wind Speed

[27] During the experiment, the change in σ_o for various rain rates was measured for 10-m neutral wind speeds that ranged from 0 to ~12 m s^{-1}. For both raining and nonraining conditions the vast majority of the data, 95%,

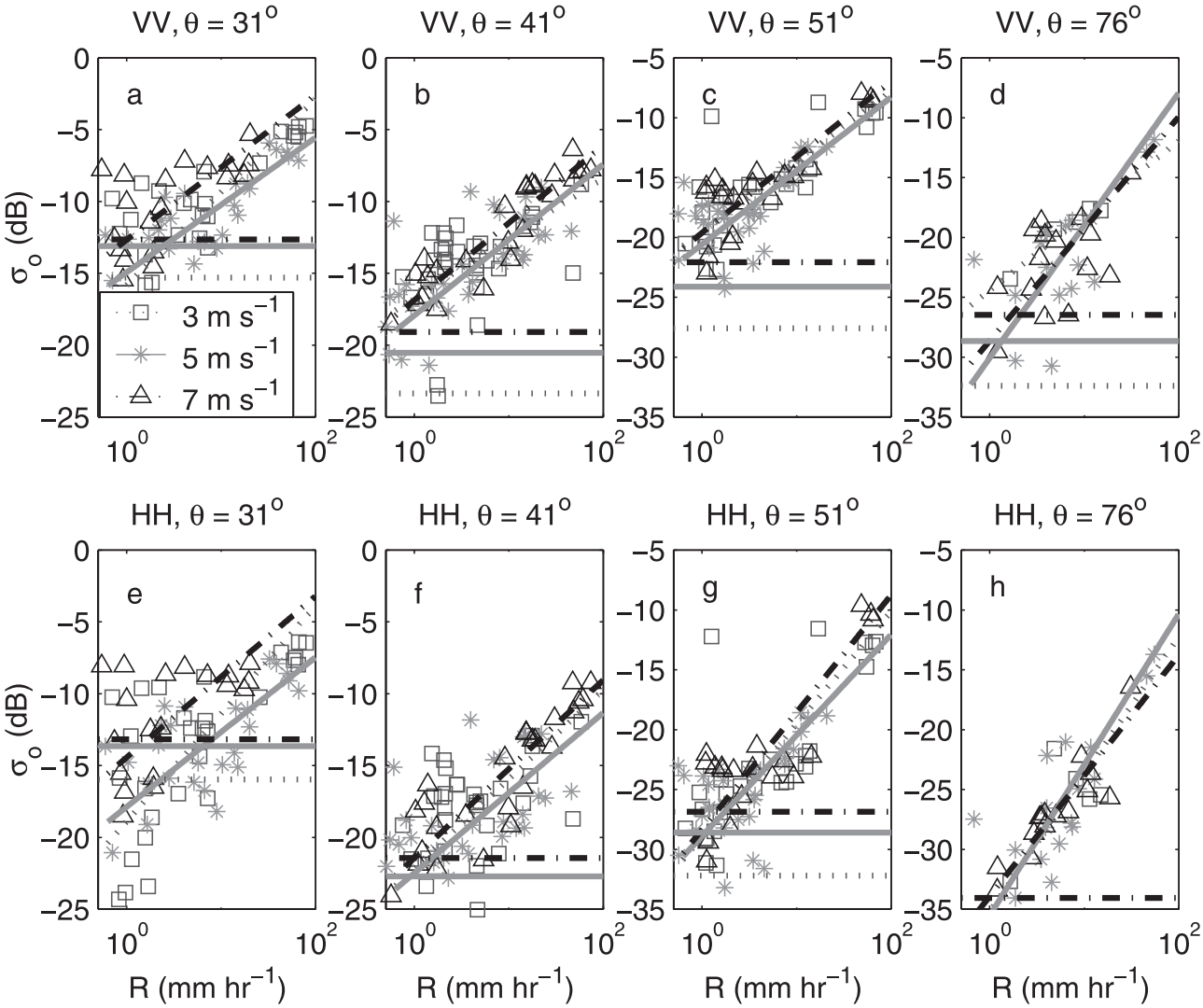

Figure 13. Cross section as a function of rain rate for wind speed bins: 2 m $s^{-1} \leq U_{10} < 4$ m s^{-1}, 4 m $s^{-1} \leq U_{10} < 6$ m s^{-1}, and 6 m $s^{-1} \leq U_{10} < 8$ m s^{-1}. Horizontal lines are the nonraining means and the diagonal are fits to the rain data. The lines correspond the wind speed bins: 2 m $s^{-1} \leq U_{10} < 4$ m s^{-1} (dotted line), 4 m $s^{-1} \leq U_{10} < 6$ m s^{-1} (solid line), and 6 m $s^{-1} \leq U_{10} < 8$ m s^{-1} (dash-dotted line).

was collected for wind speeds between 2 and 8 m s^{-1}, the most common wind speed being ~5 m s^{-1}. The effect of rain on Ku-band backscatter as a function of wind speed is shown, first for low incidence angles in Figure 10, and then for the higher incidence angles in Figure 11. The figures show the binned means in U_{10} and the associated standard errors at various incidence angles for both polarizations. The wind speed bin widths are 2 m s^{-1}. Because of the large number of nonraining samples the error bars are often so small that they are obscured by the size of the symbol. Figure 10 shows data for incidence angles, 14° and 16°, and 20°. At these angles, most of the raining mean cross sections show a decrease compared to the nonraining means; however, for both polarizations only the cross sections during rain at the 5 m s^{-1} and 7 m s^{-1} bins can be considered statistically different from their counterparts in clear conditions. At the 20° incidence angle, mean cross sections during rainfall are not statistically different from means under clear conditions.

[28] As shown in Figure 11, at incidence angles greater than about 30°, rain increases σ_o. Starting at 31° (Figures 11a and 11e), rain rates greater than 5 mm hr^{-1} show increases for the entire range of wind speeds measured during KWAJEX. As the rain rate increases so do the changes in cross section, with the greatest increases occurring at high rain rates and low wind speeds. With increasing wind speed, the magnitude of the change lessens. This result is consistent with the idea that as the wind speed increases the wind becomes more important as the source of surface scatterers. It follows that at some high wind speed the scatterers created by the wind dominate those created by the rain and the effect of rain is negligible. This wind speed transition was noted by *Braun et al.* [1999] to be between 7 m s^{-1} and 10 m s^{-1} depending on the incidence angle. We note a similar, although higher wind speed value. As the incidence angle increases to 41° (Figures 11b and 11f), 51° (Figures 11c and 11g), and 76° (Figures 11d and 11h), the magnitude of

the change grows. At 41° the maximum change, which occurs at low wind speed and heavy rain is greater than 9 dB for both polarizations; at 51° the change is greater than 12 dB; and at 76° the change is in excess of 20 dB. Interestingly, for wind speeds below the transition wind speed, σ_o appears to be independent of the wind speed when it is raining.

[29] In addition, there is a systematic difference in the scattering for the two polarizations for incidence angles equal to and greater than 41°. The increase in cross section over nonraining conditions is similar for the two polarizations at low rain rates, but for moderate and high rates the HH cross sections appear to increase more above their nonraining values than do the VV cross sections. The difference is probably due to the nature of the surface scatterers, and will be discussed later.

3.4. Cross Section Versus Rain Rate

[30] The dependence of the cross section on rain rate at low incidence angles is shown in Figure 12 while that at higher incidence angles is shown in Figure 13. The different symbols correspond to measurements with the different wind speed categories: 2 m $s^{-1} \leq U_{10} < 4$ m s^{-1}, 4 m $s^{-1} \leq U_{10} < 6$ m s^{-1}, and 6 m $s^{-1} \leq U_{10} < 8$ m s^{-1}. The horizontal lines are the non-raining mean cross sections for these wind speeds.

[31] In Figure 12, the 14° and 16° incidence angles show a substantial decrease in the cross section much of the time. Furthermore, at 14°, σ_o appears to be changed the most by light rain, with this change decreasing with rain rate. At 20°, rain has no systematic effect on the cross section.

[32] The dependence of the cross section on rain rate at the higher incidence angles is shown in Figure 13. Also plotted are functional fits to the data. The function used for the fit was a power of the form: $\sigma_o = aR^b$. This form was chosen because the data appear to be linear when σ_o, given in dB, is plotted versus log(R). A linear least squares method that minimized the perpendicular distance from the data to the line was used. At the incidence angles shown in Figure 13, the cross sections measured for both polarizations increase with rain rate.

[33] The rate of this change increases as the incidence angle grows. The values of the coefficients, a and b, as well as the fraction of the variance explained by the fit r^2, are shown in Table 1. As the rain rate decreases to zero, an accurate model would be expected to go to the mean non-raining value. However, this is a simple objective fit and it is not expected to model the low rain rates. No obvious differences are apparent in the fits at different wind speeds. Thus, within the precision of our measurements and at these wind speeds, the effect of rain on surface scattering is independent of the wind speed. The exponential form of the fit was also used by *Bliven et al.* [1997], which enables us to compare our results to theirs in Figure 14.

[34] The results of our fits at an incidence angle of 31° compare reasonably well with the measurements and model of *Bliven et al.* [1997], which were measured at an incidence angle 30°. The differences, which were mostly less than 2 dB, may be the result of the calibration of the systems or differences between laboratory and real world conditions.

Table 1. Coefficients a and b for Least Squares Fits to the Function, $\sigma_o = aR^{ba}$

	a_{VV}	b_{VV}	r_{log}^2	a_{HH}	b_{HH}	r_{log}^2
			θ = 31°			
u = 3	0.0262	0.6492	0.90	0.0129	0.7511	0.86
u = 5	0.0330	0.4593	0.94	0.0330	0.5077	0.89
u = 7	0.0557	0.4585	0.89	0.0373	0.4837	0.80
u = all	0.0364	0.5317	0.88	0.0184	0.6331	0.80
			θ = 41°			
u = 3	0.0205	0.4548	0.83	0.0060	0.6483	0.78
u = 5	0.0160	0.5405	0.90	0.0056	0.5799	0.84
u = 7	0.0197	0.5266	0.96	0.0067	0.6129	0.93
u = all	0.0364	0.5584	0.91	0.0184	0.6804	0.87
			θ = 51°			
u = 3	0.0112	0.5870	0.91	0.0013	0.9418	0.88
u = 5	0.0093	0.6028	0.87	0.0012	0.9388	0.85
u = 7	0.0095	0.6993	0.90	0.0014	0.9859	0.90
u = all	0.0103	0.5835	0.91	0.0014	0.9058	0.89
			θ = 76°			
u = 3	0.0036	0.6244	0.99	0.0003	1.1502	0.81
u = 5	0.0010	1.1089	0.82	0.0003	1.2609	0.89
u = 7	0.0014	0.9372	0.77	0.0004	1.0091	0.95
u = all	0.0015	0.8823	0.81	0.0004	1.0412	0.90

[a]For each range of wind speeds: 2 m s^{-1} to 4 m s^{-1}, 4 m s^{-1} to 6 m s^{-1}, 6 m s^{-1} to 8 m s^{-1}, and all wind speeds, the fit was computed at the incidence angles, 31°, 41°, 51°, and 76°.

[35] As mentioned in section 3.3, the increase due to rain is different for the two polarizations. Table 1 shows that for the incidence angles: 31°, 41°, 51°, and 76°, the b coefficient is greater for HH-polarization for all wind speed conditions. This means that rain has a greater effect on HH-polarized cross sections. As noted by *Braun et al.* [1999], VV polarized scatter is primarily from the ring waves, whereas HH polarized scatter is from the ring waves at low incidence angles and from stalks at large incidence angles. The intensities of these two splash products are likely to be quite different functions of the rain rate, and therefore, the difference in scattering noted in Table 1 is not surprising.

4. Conclusion

[36] The shipboard data collected during KWAJEX have illuminated some aspects of the effects of rain on Ku band backscatter from the ocean surface. Although the KWAJEX data were reliable only down to incidence angles of about 13.5°, some decrease in cross section was noted at 14°. As the incidence angle approached 20°, the effect of rain decreased to virtually none. At the moderate incidence angles where Bragg scattering dominates, the effect of rain was clearly to increase the cross section, the increase being more pronounced at higher rain rates. Cross sections measured during rain were found to be independent of wind speed below 10 m s^{-1} at all rain rates to within our experimental uncertainty. The implication for Ku-band scatterometry is that wind speed cannot be measured for winds speeds below 10 m s^{-1} when rain fills the entire surface footprint. It is important to keep in mind that both rain and wind speed can have substantial variations over the typical scatterometer footprint and that it may be

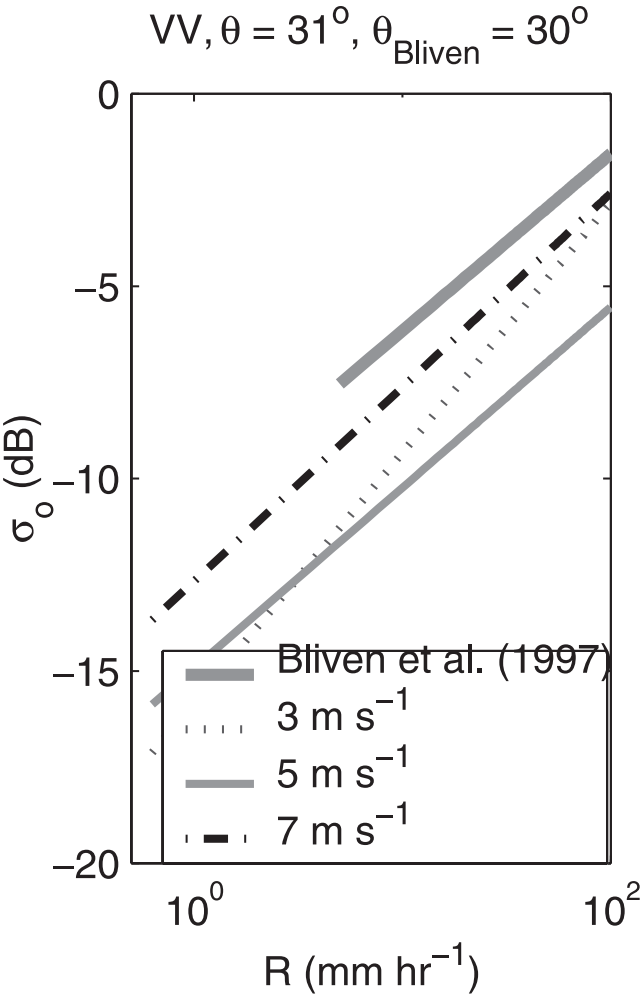

Figure 14. Fits of the cross section as a function of rain rate for wind speed bins: 2 m $s^{-1} \leq U_{10} < 4$ m s^{-1}, 4 m $s^{-1} \leq U_{10} < 6$ m s^{-1}, and 6 m $s^{-1} \leq U_{10} < 8$ m s^{-1}. The form of the fits is $\sigma_o = aR^b$.

possible to infer mean wind characteristics when there is only partial coverage by rain or the wind speed is greater than 10 m s^{-1}.

[37] Limitations of the present data set include having no data at very low incidence angles, having little data above 12 m s^{-1}, and having data at a limited range of azimuth angles. We will attempt to correct these limitations in future work. A secondary result of this work is that power scattered from rain drops and received by our CW systems yields a measure of rain rate. This feature may be helpful in experiments where auxiliary measurements of rainfall are not available. Finally, it is interesting to speculate on the nature of the scattering from an ocean surface modified by rainfall. If most of the VV polarized backscatter is due to Bragg scattering at moderate incidence angles, then the rate of change of σ_o with incidence angle is an indication of the rate of change of the surface wave spectrum with wavenumber. Figure 7 shows that this rate is much smaller in magnitude than that of a rain-free surface roughened by a 5 m s^{-1} wind. This indicates that rain roughens the ocean surface on small scales much more than moderate wind does. Rain's effect on the longer scales cannot be determined well from our present data set due to our relatively high microwave frequency and the lack of data at low incidence angles. Of course, in considering backscatter from the rain-roughened ocean, consideration must also be given to the scattering effects of splash products other than ring waves.

[38] **Acknowledgments.** The authors are grateful to Jeff Otten for helping to keep the system running during the KWAJEX cruise. We also thank Jeffrey Hare and Christopher Fairall for providing the flux data and Sandra Yuter for supplying the rain data from the cruise. This work has been supported by NASA grant NAG5-7886 and ONR grant N00014-97-1-0708.

References

Atlas, D., Footprints of storms on the sea: A view from spaceborne synthetic aperture radar, *J. Geophys. Res.*, *99*, 7961–7969, 1994.

Bliven, L. F., P. W. Sobieski, and C. Craeye, Rain generated ring-waves: Measurement and modeling for remote sensing, *Int. J. Remote Sens.*, *18*(1), 221–228, 1997.

Braun, N., M. Gade, and P. A. Lange, Radar backscattering measurements of artificial rain impinging on a water surface at different wind speeds, paper presented at 1999 International Geoscience and Remote Sensing Symposium (IGARSS), Inst. of Elect. and Elect. Eng., New York, 1999.

Businger, J. A., J. C. Wyngaard, Y. Izumi, and E. F. Bradley, Flux profile relationships in the atmospheric surface layer, *J. Appl. Meteorol.*, *28*, 181–189, 1971.

Capolino, F., L. Facheris, D. Giuli, and F. Sottili, The determination of the sea surface NRCS when corrugated by blowing wind and rainfall: An application of rainfall rate measurements over sea, paper presented at 10th International Conference on Antennas and Propagation, Inst. of Elect. Eng., London, 1997.

Dyer, A. J., A review of the flux-profile relationships, *Boundary Layer Meteorol.*, *7*, 363–372, 1974.

Gade, M., N. Braun, and P. A. Lange, Laboratory measurements of artificial rain impinging on a wind-roughened water surface, paper presented at 1998 International Geoscience and Remote Sensing Symposium (IGARSS), Inst. of Elect. and Elect. Eng., New York, 1998.

Garratt, J. R., *The Atmospheric Boundary Layer*, Cambridge Univ. Press, New York, 1992.

Gunn, R., and G. D. Kinzer, The terminal velocity of fall for water drops in stagnant air, *J. Meteorol.*, *6*, 243–248, 1949.

Haddad, Z. S., A. R. Jameson, E. Im, and L. Durden, Improved coupled Z-R and k-R relations and the resulting ambiguities in the determination of the vertical distribution of rain from the radar backscatter and the integrated attenuation, *J. Appl. Meteorol.*, *34*, 2680–2688, 1995.

Hansen, J. P., Rain backscatter tests dispel old theories, *Microwaves RF*, *6*, 97–102, 1986.

Hasse, L., M. Grossklaus, K. Uhlig, and P. Timm, A ship rain gauge for use in high wind speeds, *J. Atmos. Oceanic Technol.*, *15*, 380–386, 1998.

Marshall, J. S., and W. M. Palmer, The distribution of raindrops with size, *J. Meteorol.*, *5*, 165–166, 1948.

Méhauté, B. L., Gravity-capillary rings generated by water drops, *J. Fluid Mech.*, *197*, 415–427, 1988.

Melsheimer, C., W. Alpers, and M. Gade, Investigation of multifrequency/multipolarization radar signatures of rain cells over the ocean using SIR-C/X-SAR data, *J. Geophys. Res.*, *103*, 18,867–18,884, 1998.

Miller, S., C. Friehe, T. Hristov, J. Edson, and S. Wetzel, Wind and turbulence profiles in the surface layer over ocean waves, in *Wind-Over-Wave Couplings: Perspectives and Prospects, Salford University, England*, Salford Univ., Southend-on-Sea, England, 1997.

Moore, R. K., Y. S. Yu, A. K. Fung, D. Kaneko, G. J. Dome, and R. E. Werp, Preliminary study of rain effects on radar scattering from water surfaces, *IEEE J. Oceanic Eng.*, *4*(1), 31–32, 1979.

Nystuen, J. A., A note on the attenuation of surface gravity waves by rainfall, *J. Geophys. Res.*, *95*, 18,353–18,355, 1990.

Plant, W. J., E. A. Terray, J. Robert, A. Petitt, and W. C. Keller, The dependence of microwave backscatter from the sea on illuminated area: Correlation times and lengths, *J. Geophys. Res.*, *99*, 9705–9723, 1994.

Plant, W. J., W. C. Keller, V. Hesany, K. Hayes, K. W. Hoppel, and T. V. Blanc, Measurements of the marine boundary layer from an airship, *J. Atmos. Oceanic Technol.*, *15*, 1433–1458, 1998.

Smith, M. J., E. M. Poulter, and J. A. McGregor, Doppler radar backscatter from ring waves, *Int. J. Remote Sens.*, *19*(2), 295–305, 1998.

Sobieski, P. W., C. Craeye, and L. F. Bliven, Scatterometric signatures of multivariate drop impacts on fresh and salt water surfaces, *Int. J. Remote Sens.*, *20*(11), 2149–2166, 1999.

Tsimplis, M. N., The effect of rain in calming the sea, *J. Phys. Oceanogr.*, *22*, 404–412, 1992.

Wentz, F. J., S. Peteherych, and L. A. Thomas, A model function for ocean radar cross sections at 14.6 GHz, *J. Geophys. Res.*, *89*, 3689–3704, 1984.

Wetzel, L. B., On the theory of electromagnetic scattering from a raindrop splash, *Radio Sci.*, *25*(6), 1183–1197, 1990.

Worthington, A. M., *A Study of Splashes, Including His 1894 Lecture: The Splash of a Drop and Allied Phenomena*, Macmillan, New York, 1963.

Yang, Z., S. Tang, and J. Wu, An experimental study of rain effects on fine structures of wind waves, *J. Phys. Oceanogr.*, *27*, 419–430, 1997.

R. F. Contreras, Department of Atmospheric Sciences, University of Washington, 408 Atmospheric Sciences-Geophysics (ATG) Building, Box 351640, Seattle, WA 98195-1640, USA. (drobb@u.washington.edu)

K. Hayes, W. C. Keller, J. Nystuen, and W. J. Plant, Applied Physics Laboratory, University of Washington, 1013 NE 40th Street, Box 355640, Seattle, WA 98105-6698, USA. (hayes@apl.washington.edu; keller@apl.washington.edu; nystuen@apl.washington.edu; plant@apl.washington.edu)